Heliyon 8 (2022) e12034

Contents lists available at ScienceDirect

Heliyon

journal homepage: www.cell.com/heliyon

Research article

Concurrent investigation of antimony chalcogenide (Sb_2Se_3 and Sb_2S_3)-based solar cells with a potential WS_2 electron transport layer

Md. Ferdous Rahman [a,b,**], Md. Mahabub Alam Moon [a,***], M. Khalid Hossain [c,d,*], Md. Hasan Ali [a], Md. Dulal Haque [e], Abdul Kuddus [b,f], Jaker Hossain [b], Abu Bakar Md. Ismail [b]

[a] Department of Electrical and Electronic Engineering, Begum Rokeya University, Rangpur 5400, Bangladesh
[b] Solar Energy Laboratory, Department of Electrical and Electronic Engineering, University of Rajshahi, Rajshahi 6205, Bangladesh
[c] Institute of Electronics, Atomic Energy Research Establishment, Bangladesh Atomic Energy Commission, Dhaka 1349, Bangladesh
[d] Department of Advanced Energy Engineering Science, Interdisciplinary Graduate School of Engineering Science, Kyushu University, Fukuoka 816-8580, Japan
[e] Department of Electronics and Communication Engineering, Hajee Mohammad Danesh Science and Technology University, Dinajpur 5200, Bangladesh
[f] Graduate School of Science and Engineering, Saitama University, Saitama 338-8570, Japan

HIGHLIGHTS

- Antimony chalcogenide (Sb_2Se_3 and Sb_2Se_3)-based TFSCs with WS_2 electron transport layer were studied by SCAPS-1D simulator.
- Systematic investigation on the impacts of thickness, doping, bulk, and interface defect densities on the PV performance.
- PCE of 28.20% (26.60%) was found in a 1280 nm thick $n^+/n/p$ junction Sb_2Se_3 (Sb_2S_3) solar cell under adjusted condition.
- The simulation was verified with the Shockley–Queisser (SQ) limit including experimental as well as simulation works.

GRAPHICAL ABSTRACT

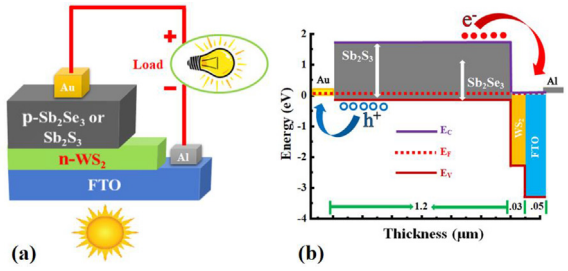

ARTICLE INFO

Keywords:
Heterojunction solar cell
Sb_2Se_3
Sb_2S_3
WS_2 electron transport layer
SCAPS-1D

ABSTRACT

Antimony (Sb) chalcogenides such as antimony selenide (Sb_2Se_3) and antimony sulfide (Sb_2S_3) have distinct properties to be used as absorber semiconductors for harnessing solar energy including high absorption coefficient, tunable bandgap, low toxicity, phase stability. The potentiality of Sb_2Se_3 and Sb_2S_3 as absorber material in Al/FTO/Sb_2Se_3(or Sb_2S_3)/Au heterojunction solar cells (HJSCs) with 2D tungsten disulfide (WS_2) electron transport layer (ETL) layer has been investigated numerically using SCAPS-1D solar simulator. A systematic investigation of the impact of physical properties of each active material of Sb_2Se_3, Sb_2S_3, and WS_2 on photovoltaic parameters including layer thickness, carrier doping concentration, bulk defect density, interface defect density, carrier generation, and recombination. This study emphasizes the exploration of causes of low performance of actual devices and demonstrates the individual variation in the open-circuit voltage (V_{OC}), short-circuit current density (J_{SC}), fill factor (FF), power conversion efficiency (PCE) and quantum efficiency (QE). Thereby, highly potential heterostructures of Al/FTO/WS_2/absorber (Sb_2Se_3 or Sb_2S_3)/Au proposed, in which, the PCE

* Corresponding author.
** Corresponding author.
*** Corresponding author.
E-mail addresses: ferdous@brur.ac.bd (F. Rahman), mmamoon9357@gmail.com (M.A. Moon), khalid.baec@gmail.com, khalid@kyudai.jp (M.K. Hossain).

https://doi.org/10.1016/j.heliyon.2022.e12034
Received 29 July 2022; Received in revised form 26 October 2022; Accepted 25 November 2022

over 28.20 and 26.60% obtained with V_{OC} of 850 and 1230 mV, J_{sc} of 38.0 and 24.0 mA/cm^2, and *FF* of 86.0 and 89.0% for Sb_2Se_3 and Sb_2S_3 absorber, respectively. These detailed findings revealed that the Sb-chalcogenide heterostructure with potential WS_2 ETL can be used to realize the fabrication of feasible thin film solar cells and thus the design of high-efficiency high-current (HEHC) and high-efficiency high-voltage (HEHV) solar panels.

1. Introduction

Photovoltaic technologies provide a clean, eco-friendly, cost-effective, and long-term solution to meet rising worldwide energy demand by directly converting solar energy into electricity [1–5]. Different types of solar cells have been technologically advanced to meet increasing energy demands [6–9], including silicon (Si) [10–15], cadmium telluride (CdTe), copper indium gallium selenide (CIGS), copper zinc tin sulfide (CZTS), polymer, inorganic metal chalcogenide, dye-sensitized solar cell (DSSC) [16–18], quantum dot (QD), and perovskite-based solar cells [19–22].

A single-junction solar cell with a bandgap of around 1.14 eV of the absorber layer can provide the highest power conversion efficiency (PCE) of 33.3%, according to the Shockley-Queisser (SQ) model [23]. Thin-film solar cells (TFSCs) based on silicon, CIGS, and CdTe, on the other hand, have attained PCEs of over 20% [6,24,25]. Despite the abundance of Si on earth, the rarity of In, Ga, and Te, as well as the toxicity of Cd, limit their use on a broad scale, which has been one of the key challenges for CIGS and CdTe solar cells [26,27]. As a result, in the last decade, various novel earth-abundant absorber materials, such as Cu_2SnS_3 [28], Cu_2GeS_3 [29], $Cu_2(Sn,Ge)S_3$ [30], GeSe [31], $CuSbS_2$ [32], $CuSbSe_2$ [33], $Cu_2ZnSnSe_4$ [34], FeS_2 [35], $FeSi_2$ [36], SnSe [37], Sb_2Se_3 [38], and Sb_2S_3 [39], have been suggested as an alternative for the eco-friendly, and golden triangle requirements: low cost, high PCE, and long-term durability of TFSCs [1].

Among them, Sb_2Se_3 and Sb_2S_3 have attracted considerably and advanced hurriedly [39–44] due to their excellent photovoltaic properties, such as a suitable bandgap (1.1–1.7 eV) for single-junction solar cells [45], a high absorption coefficient (>10^5 cm^{-1} at visible light) [46], a low melting point (550 °C) [47], low-cost constituents [48], and low structural complexity with only one crystallographic phase [49].

To fabricate Sb_2Se solar cells, several major approaches [40,48,50] with different buffer layers [40,51,52] have been used. It's worth noting that while Sb_2Se has been investigated for more than 40 years, its usage as absorber material in solar cells has only recently become popular, with significant progress occurring since 2009. A comparative study of experimentally fabricated Sb_2Se_3-and Sb_2S_3-based heterojunction solar cells (HJSCs) are summarized in Tables S1 and S2 in the supplementary materials. Overall, the first experimental efficiency of the Sb_2Se_3 and Sb_2S_3 TFSC in 2009 was 0.66% [53] and 3.7% [54] which improved to 9.2% in 2019 [55] and 6.53% in 2020 [56], respectively. Lin et al. fabricated glass/Mo/Sb_2Se_3/CdS/ITO/Ag solar cells using the sputtering technique and delivered PCE of 7.43% [57]. In recent times, Tang et al.

Table 1. Layer properties for simulation 60, 61, 62, 63, 64, 65, 66, 67, 69, 70, 77, 78, 79].

Parameters (unit)	FTO	WS_2	Sb_2Se_3	Sb_2S_3
Thickness (nm)	50	30	1200	1200
Bandgap (eV)	3.60	2.20	1.20	1.62
Electron affinity (eV)	4	3.95	4.16	3.70
Dielectric permittivity	9	13.60	14.50	7.08
CB effective DOS (cm^{-3})	2.2×10^{18}	2.2×10^{18}	2×10^{18}	2×10^{19}
VB effective DOS (cm^{-3})	1.80×10^{19}	1.80×10^{19}	10^{19}	10^{19}
Electron mobility (cm^{2}V^{-1}s^{-1})	100	100	16.70	9.80
Hole mobility (cm^{2}V^{-1}s^{-1})	25	100	16.70	10
Donor density, N_D (cm^{-3})	5×10^{18}	10^{17} (Sb_2Se_3), 10^{18} (Sb_2S_3)	0	0
Acceptor density, N_A (cm^{-3})	0	0	10^{13}	10^{15}
Defect type	acceptor	acceptor	donor	donor
Bulk defect density, N_t (cm^{-3})	10^{14}	10^{18}	10^{12}	10^{12}
Electron capture cross-section, σ_e (cm^2)	10^{-15}	10^{-15}	10^{-15}	10^{-15}
Hole capture cross-section, σ_p (cm^2)	10^{-15}	10^{-15}	10^{-15}	10^{-15}
Defect position above E_V (eV)	0.6	0.6	0.6	0.6

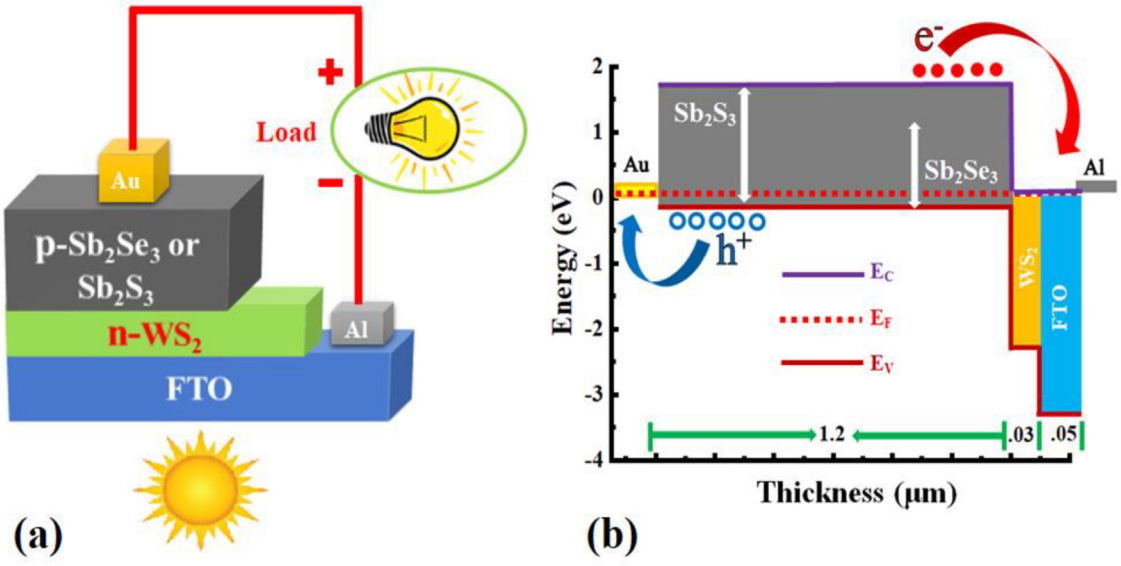

Figure 1. (a) Proposed Al/FTO/WS_2/Sb_2Se_3(or Sb_2S_3)/Au HJSC, and (b) corresponding band diagram.

Table 2. Interface parameters used in the ETL/absorber interface of the designed HJSCs.

Parameters (unit)	WS_2/Sb_2Se_3 Interface	WS_2/Sb_2S_3 Interface
Defect type	Neutral	Neutral
Electron capture cross- section, σ_e (cm^2)	10^{-19}	10^{-19}
Hole capture cross-section, σ_p (cm^2)	10^{-19}	10^{-19}
Defect position above the highest E_V (eV)	0.06	0.06
Defect density (cm^{-2})	10^{15}	10^{10}

have achieved PCE 8.64% by sputtering technique with record V_{OC} of 0.52 V [58].

However, using the SCAPS-1D simulator, multiple Sb_2Se [59–61] and Sb_2Se_3 [62] based solar cell architectures with varying electron transport layers (ETLs) [63,64] and hole transport layers (HTLs) [65,66] have recently been explored, with reasonably good photovoltaic (PV) performance. Basak et al. have recently explored the Sb_2S_3 (or Sb_2Se_3)/CdS heterojunction solar cell (HJSC) in SCAPS-1D and found PCEs of 9.51% and 12.62%, respectively, for Sb_2S_3 and Sb_2Se_3 HJSC [67]. However, according to the review of simulation-based studies on these solar cells, the maximum efficiency is 23.18% [65]. Yet their theoretical PCE is inferior to that of comparable commercial TFSCs [24,68]. Furthermore, while CdS is widely used as a window or buffer layer in PV devices due to its appropriate bandgap [69], the toxicity of Cd [70] leads researchers to continue looking for other environmentally friendly and wide bandgap materials to use as window or buffer layer in antimony (Sb) chalcogenide-based solar cells [70]. In this perspective, tungsten disulfide (WS_2) offers relaxed carrier transport by acceptable band alignment with Sb_2Se_3 and Sb_2S_3-based solar cells, while also being earth-abundant, economical, adhesive, and non-toxic [70]. Consequently, performing systematic numerical analysis in the SCAPS-1D simulator, we have designed, simulated, and proposed simplified designs for the efficiency enhancement of Sb_2Se_3 and Sb_2S_3-based solar cells employing WS_2 as ETL. Our proposed devices, with their optimized parameters, provide superior results to the devices proposed earlier [65–67].

2. Modeling and simulation

Figure 1 shows the schematic structure and band alignment of proposed Al/FTO/WS_2/Sb_2Se_3 (or Sb_2S_3)/Au HJSC structure, where FTO, WS_2, and Sb_2Se_3 (or Sb_2S_3) are used as the n^+-type window layer, n-type electron transport, or buffer layer, and the p-type active absorber layer, respectively.

In this work, a one-dimensional solar cell capacitance simulator (SCAPS-1D) of version 3.3.07 [71,72] has been used to conduct the whole investigation. Though the SCAPS simulator allows researchers to explore devices with up to seven layers [69], the current structure of the designed solar cell with only three layers has a substantial impact on PV performance, as will be described in subsequent section 3. Light travels through the FTO-coated glass substrate and WS_2 ETL and finally reaches the absorber layer in this approach. FTO is a common material for substrate in HJSCs due to its chemical and mechanical durability, thermal stability, low toxicity, and inexpensive raw material and processing costs [73,74] which is why we used this substrate to achieve a higher value for the design cell's performance to cost ratio. However, considering the practical constraints we assumed 90% transmission (visible absorption of FTO is 0.04) of light incident onto the surface of the FTO layer [69].

Since, Au is a noble metal having two major advantages: (a) chemically inert and (b) high work function metal (5.1–5.3 eV), which is required for hole extraction efficiently at the back interface in p-type absorbers (VBM of 5.36 eV) forming ohmic contact, Au was chosen as back metal contact. J. Zhang et al reported that the forward current in Sb_2Se_3 solar cells with Al(WF of 4.0–4.2 eV) back contact is very low even under large forward bias (0.2 mA/cm^2 at 1 V, owing to a large barrier at the back interface for hole extraction and consequently blocking current across the solar cell significantly [75]. Although they proposed NiO_x/Ni as a promising one alike Au as back contact, Au was preferred to investigate the efficacy of the absorber and ETL layer in detail with no use of

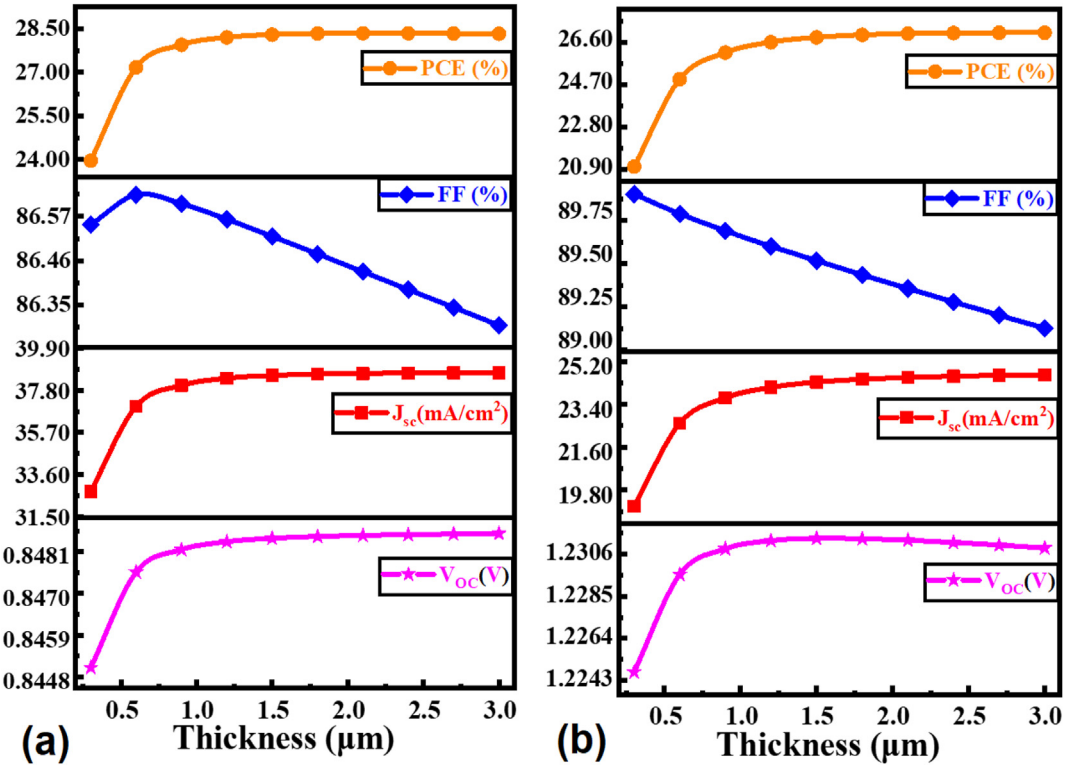

Figure 2. Effect of absorber layer thickness (a) Sb_2Se_3 and (b) Sb_2S_3 on the PV parameters.

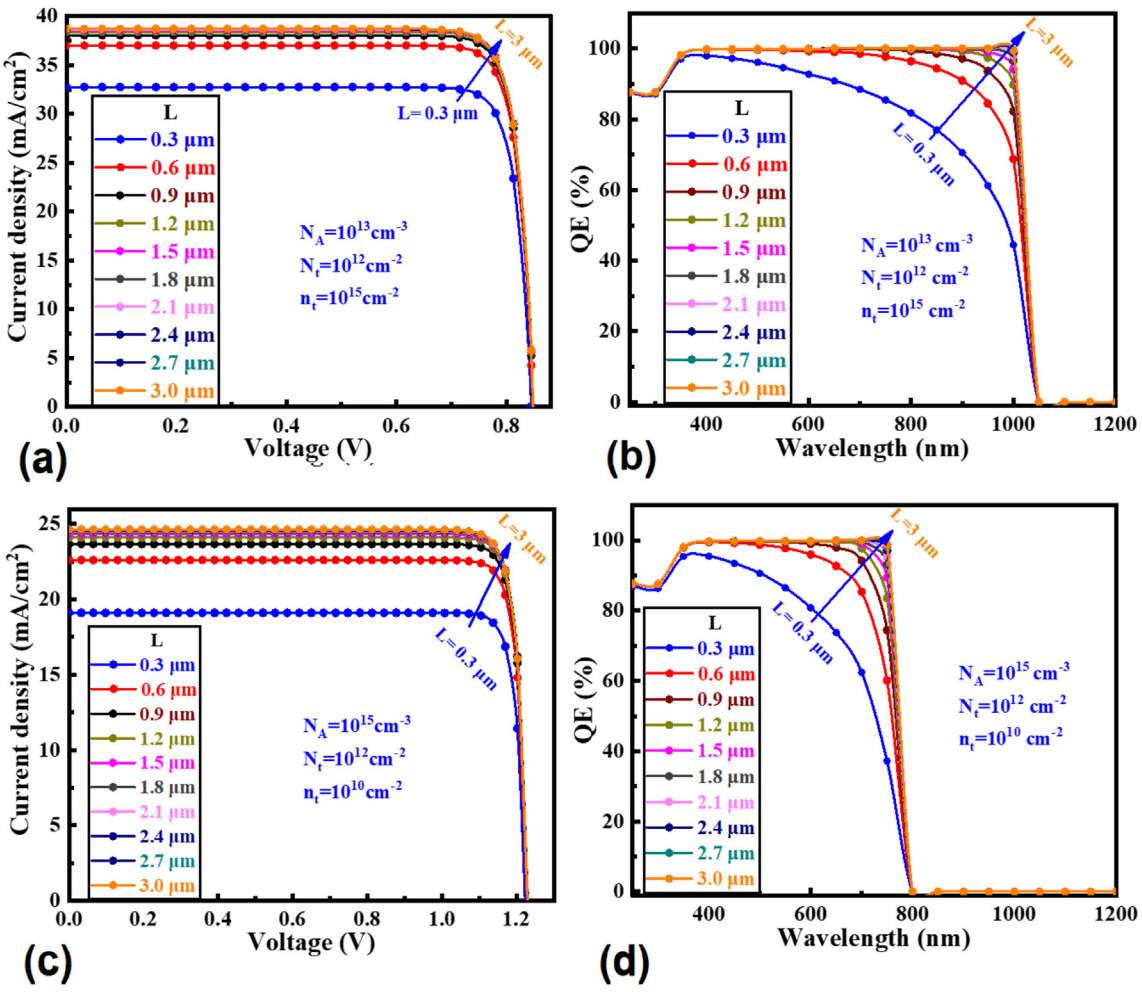

Figure 3. Impact of the absorber layer thickness of (a, b) Sb_2Se_3, and (c, d) Sb_2S_3 solar cells on the JV and QE, respectively.

HTL or any HTL like NiO_x as recommended. On the other hand, Al (WF of 4.0–4.2 eV) was used as a front metal electrode with FTO (4.0 eV) considering both the work function for obtaining ohmic contact and its availability. Since, Aluminum is the most abundant metal on Earth, as well as one of the cheapest metals, therefore, Al was chosen as the front metal contact with FTO TCO.

Nevertheless, SCAPS-1D software was developed based on the semiconductor principal equations and is largely used to model semiconductor solar cells [71]. More particularly, the Poisson, hole, and electron continuity equations are employed to determine the numerical assessments of the modeled solar cell structure, as shown in Eqs. (1), (2), and (3), respectively [65,76].

$$\frac{\partial^2 \Psi}{\partial x^2} + \frac{q}{\varepsilon}\left[p(x) - n(x) + N_D + N_A + \rho_p - \rho_n\right] = 0 \tag{1}$$

$$\frac{1}{q}\frac{\partial J_p}{\partial x} = G_{op} - R(x) \tag{2}$$

$$\frac{1}{q}\frac{\partial J_n}{\partial x} = -G_{op} + R(x) \tag{3}$$

where, Ψ, q, ε, N_A (N_D), and ρ_p (ρ_n) denote electrostatic potential, the charge of an electron, dielectric permeability, hole (electron) concentration, and hole (electron) distribution, respectively. In addition, J_P (J_n), G_{OP}, R, and p (n) present current density contributed by hole (electron), optical carrier generation rate, recombination rate, and free acceptor (donor) concentration, respectively.

The drift-diffusion formulas of Eqs. (4) and (5) have been used to calculate the transport properties of the donor and acceptor of semiconducting material [65,76].

$$J_p = \frac{\mu_p p}{q}\frac{\partial E_{FP}}{\partial x} \tag{4}$$

$$J_n = \frac{\mu_n n}{q}\frac{\partial E_{Fn}}{\partial x} \tag{5}$$

where, μ_P (μ_n) and E_{FP} (E_{Fn}) specify the acceptor (donor) mobility and acceptors' (donors') fermi level, respectively.

The designed solar cell has been simulated under global air mass (AM) 1.5 spectrum at a one sun illumination (100 mW/cm^2) at a temperature T = 300 K. The thermal velocity of electron and hole was set to 10^7 cm/s and kept constant throughout the entire simulation. Tables 1 and 2 show all other necessary layer properties of Sb_2Se_3-and Sb_2S_3-based HJSCs that are necessary for conducting the whole simulation [60–67,69,70,77,78].

3. Result and discussions

3.1. Impact of the absorber layer on the PV performance

3.1.1. Thickness effect

Figure 2 shows the influence of thickness variation on the solar cell performance parameters in the range of 0.3–3.0 μm at constant values of the rest all other parameters as declared in Tables 1 and 2 at 300 K. The

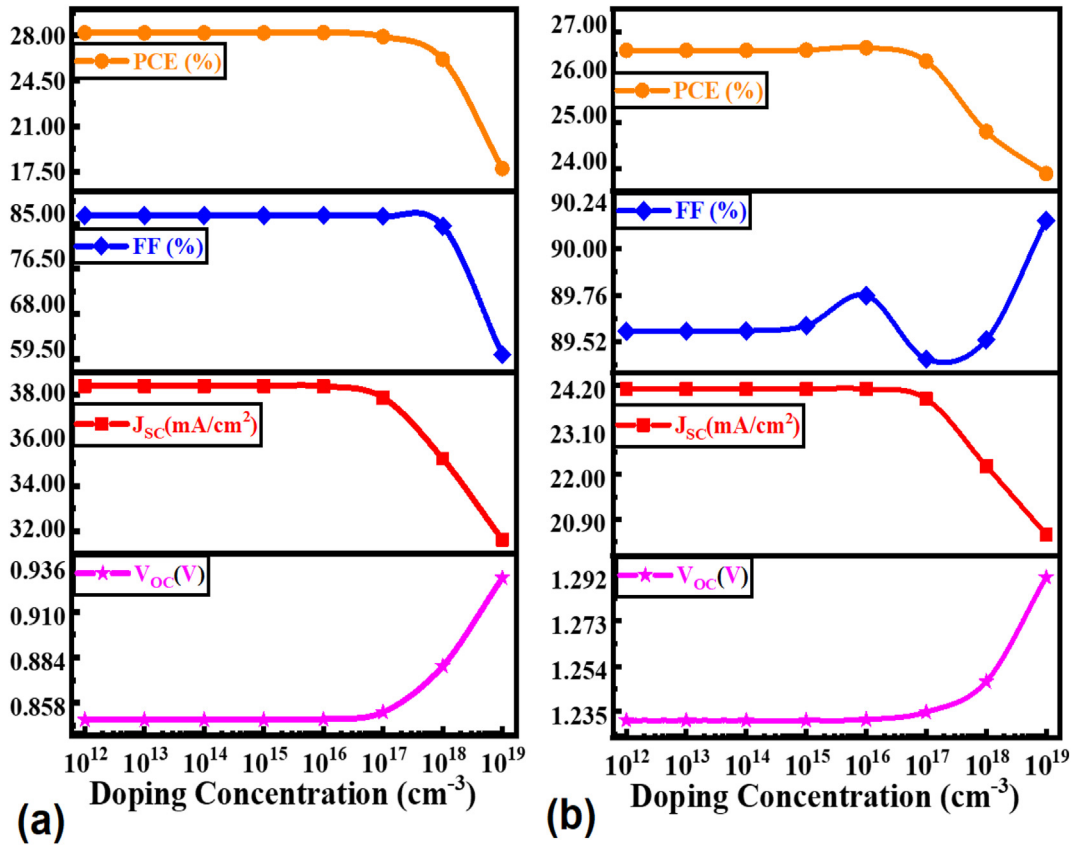

Figure 4. Effect of the doping concentration of (a) Sb_2Se_3, and (b) Sb_2S_3 absorber layer on the solar cell performance parameters.

cell's PCE increased from 23.9 to 28.5% and 20.9 to 26.6 with the increase of Sb_2Se_3 and Sb_2S_3 absorber thickness from 0.3– 3.0 μm, respectively. The J_{sc} increased linearly first in both devices corresponding to the absorber layer thickness of ≤0.75 μm and then it reached a saturated value of 38 and 24 mA/cm^2, in contrast, the FF tends to decrease almost linearly for Sb_2Se_3 and Sb_2S_3 absorber, respectively. This increment of J_{sc} is owing to the marked improvement of photon absorption at thicker Sb_2Se_3 or Sb_2S_3 absorber layer. This is reasonable because a thicker absorber has a greater number of photons to produce higher electron-hole pairs (EHPs) [69,80].

In Figure 3, the quantum efficiency (QE) response of the corresponding solar cells at different absorber thicknesses also reveals similar consequences as observed in J_{sc}. Further, an increase of cell resistance, as well as diffusion length at thicker absorber layer, causes the decrease of FF [69,81]. In addition, a negligible change in V_{oc} from 0.845– 0.848 V and 1.22–1.23 V for Sb_2Se_3 and Sb_2S_3 absorbers are observed, respectively. Thus, the highest PCE of 28.5 and 26.6% were observed at a Sb_2Se_3 and Sb_2S_3 absorber thickness of 1.2 μm at adjusted photovoltaic parameters values, which is chosen for further investigation.

3.1.2. Doping concentration effect

Figure 4 illustrates the impact of doping concentration N_A of Sb_2Se_3 and Sb_2S_3 absorber layer varied in the range of 10^{12}–10^{19} cm^{-3} at 300 K on the solar cell parameters at a constant value of the rest others parameters as summarized in Tables 1 and 2. The change of each output parameter was affected negligibly by varied N_A to a value of 10^{17} cm^{-3}. The J_{sc} dropped significantly from ~39.0 to 31.0 mA/cm^2 and ~25.0 to 20.0 mA/cm^2 and FF reduced from 85.0 to 59.0% and 85.0 to 59.0%, in contrast, V_{oc} increased from 840 to 930 mV and 1230–1295 mV for Sb_2Se_3 and Sb_2S_3 absorber respectively. The decrease of photocurrent at higher acceptor concentration owing to the domination of recombination of photogenerated hole pairs at higher carrier density. The increase of V_{oc} originated from the improved build-in-potential by further lowering fermi-level at higher acceptor concentration and thereby larger band offset compare with lower doping level at the absorber/buffer interface. Therefore, a sharp decrease in J_{SC} and therefore the PCE is observed. By adjusting the PV parameters value, the optimum N_A was found at 10^{13} and 10^{15} cm^{-3} for Sb_2Se_3 and Sb_2S_3 absorbers, respectively. Thus, the PCE of 28.20 and 26.6%, V_{OC} of 840 and 1230 mV, J_{SC} of 38.40 and 24.11 mA/cm^2, FF of 86.55 and 89.6% at an optimum N_A value for Sb_2Se_3 and Sb_2S_3 absorbers, respectively.

Figure 5 shows the impact of the doping concentration of Sb_2Se_3 and Sb_2S_3 absorber layers on the JV and QE spectra of the corresponding solar cells, respectively. The response of QE reduces markedly in the case of both absorber configurations when the hole doping level exceeds 10^{17} cm^{-3} which further reveals the recombination of the photogenerated carrier as expected from an increase in the recombination of free carrier charges within the bulk. The lower energy (longer wavelength) photons are absorbed noticeably in the absorber layer. Consequently, a dramatic impact of the doping concentration on the collected conversion efficiency was observed [82].

3.1.3. Effect of the carrier concentration of the absorber layer on the G-R profile

Figure 6 demonstrates the influence of carrier (electron and hole) concentration and total generation-recombination (G-R) profiles as a function of Sb_2Se_3 and Sb_2S_3 absorber layer thickness. The effective density of states (DOS) in the valence bands, the hole concentration of Sb_2S_3 is slightly larger than that of Sb_2Se_3 owing to the difference in acceptor concentration in the absorbers, and. In contrast, the electron concentration of the Sb_2S_3 absorber is lower than that of the Sb_2Se_3 absorber. The carrier generation and recombination profiles obtained by a systematic study revealed the potentiality of each Sb-chalcogenides-based absorber of Sb_2S_3 and Sb_2Se_3 compare with reported inorganic,

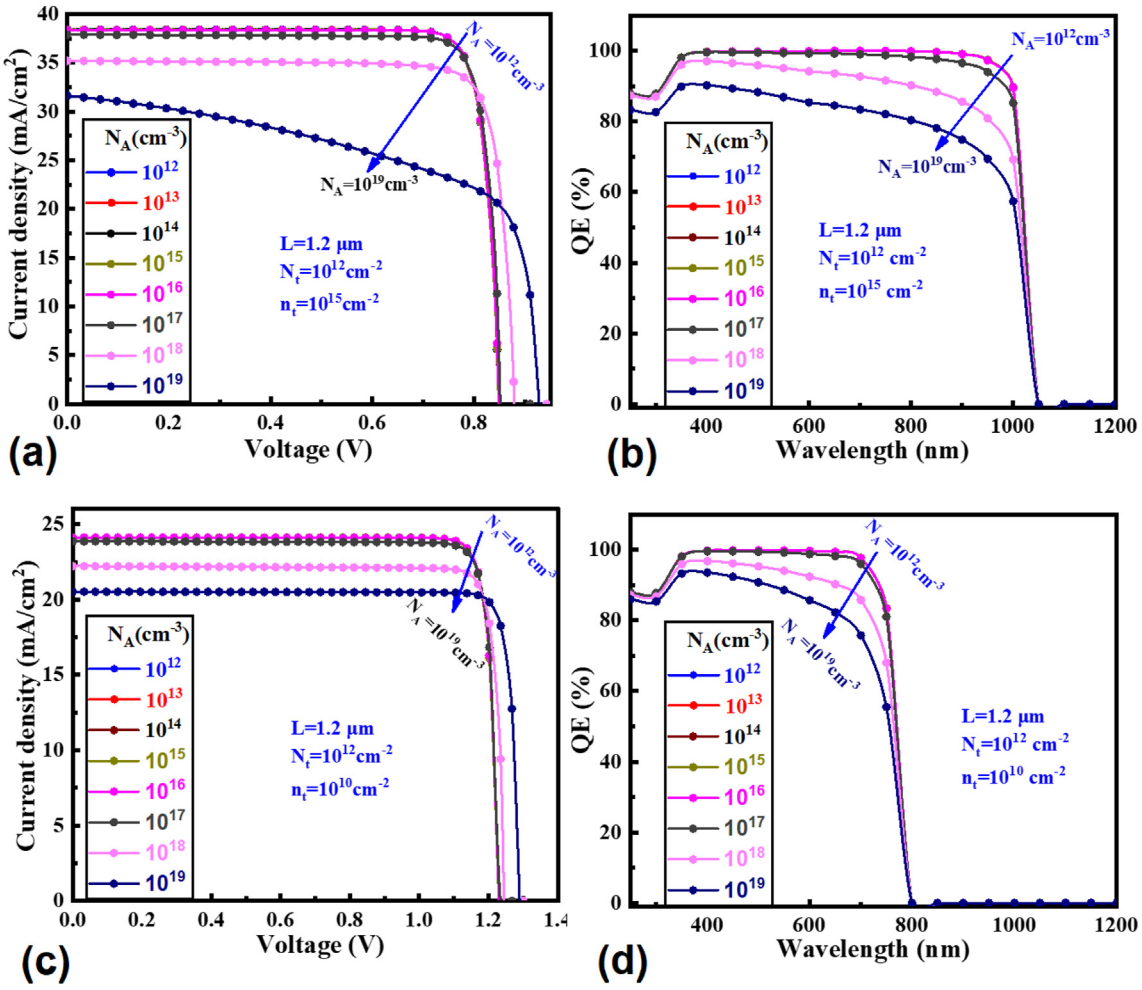

Figure 5. Impact of the absorber layer doping concentration of (a, b) Sb_2Se_3, and (c, d) Sb_2S_3 solar cells on the JV and QE, respectively.

organic, and compound semiconductor materials used as an absorber at a specified and adjusted carrier concentration and defect density [83–87]. Thus, Sb-chalcogenides-based Sb_2S_3 and Sb_2Se_3 appear of much more promising and efficient absorber materials, which can be used for the fabrication of high-performance thin film solar cells with lower e-h recombination, in contrast, higher carrier generation.

3.2. Impact of WS_2 ETL layer on the photovoltaic performance

Figure 7 shows the effect of thickness and doping concentration of WS_2 ETL on the performance of Sb_2Se_3-based solar cell devices in the range of 0.01–0.21 μm and 10^{14}–10^{21} cm^{-3} respectively, keeping unchanged all other associated parameters as summarized in Tables 1 and 2. The V_{OC} increases from 0.8483 to 0.9293 V, while the J_{SC} decreases from 38.40 to 31.63 mA/cm^2 with an increase of donor concentration from 10^{12} to 10^{19} cm^{-3}. The increment of V_{OC} originated from the improved electric field with higher resultant V_{bi} developed at higher donor concentration in WS_2 ETL. On the other hand, the availability of a higher density of carriers causes a larger recombination rate of photogenerated carriers, consequently reducing J_{SC} [88,89]. In addition, an insignificant impact of donor concentration on FF was observed. However, fewer photons may reach the absorber layer when the ETL thickness increases, resulting in a reduction in EHP generation due to parasitic absorption by the ETL itself. Consequently, the JSC and the PCE of both the solar cells tend to decrease [36, 69,81]. Thus, the highest PCE of ~29.0% was observed at WS_2 ETL thickness of ~0.03 μm and carrier concentration of $\leq 10^{17}$ cm^{-3}.

Figure 8 demonstrates the impact of thickness and doping concentration of WS_2 ETL on the performance of Sb_2S_3-based solar cells in the range of 0.01–0.21 μm and 10^{14}–10^{21} cm^{-3} respectively, at a constant of all other parameters as summarized in Tables 1 and 2. The V_{OC} increases from 1.21 to 1.23 V, in contrast, the J_{SC} decreases from 24.11 to 20.52 mA/cm^2 with the increase of donor concentration from 10^{12} to 10^{19} cm^{-3}. The increment of V_{OC} originated by the improved electric field with enhanced resultant V_{bi} developed at higher donor concentration in WS_2 ETL as observed in the case of Sb_2S_3-based cells. On the other hand, higher carrier density causes increased recombination of photogenerated carriers, consequently, reduced J_{SC} observed. The photons of longer wavelengths are deeply absorbed in the absorber layer at higher doping concentration owing to a smaller mean free path at a higher carrier density state.

Thus, the optimum thickness of WS_2 ETL was found of 0.03 μm with a donor concentration of 10^{17} and 10^{18} cm^{-3} for both Sb_2Se_3 and Sb_2S_3 absorber-based heterostructures, respectively, considering the tradeoff condition among solar cell parameters.

3.3. Influence of the bulk and interface defect density on the PV performance

Defects are mainly originated from dislocations and grain boundaries (GBs) in the synthesized layers. The defect density reduces the carrier lifetime and mobility markedly, which in turn acts as a carrier trapping center or carrier recombination [90]. Thus, cell performance is

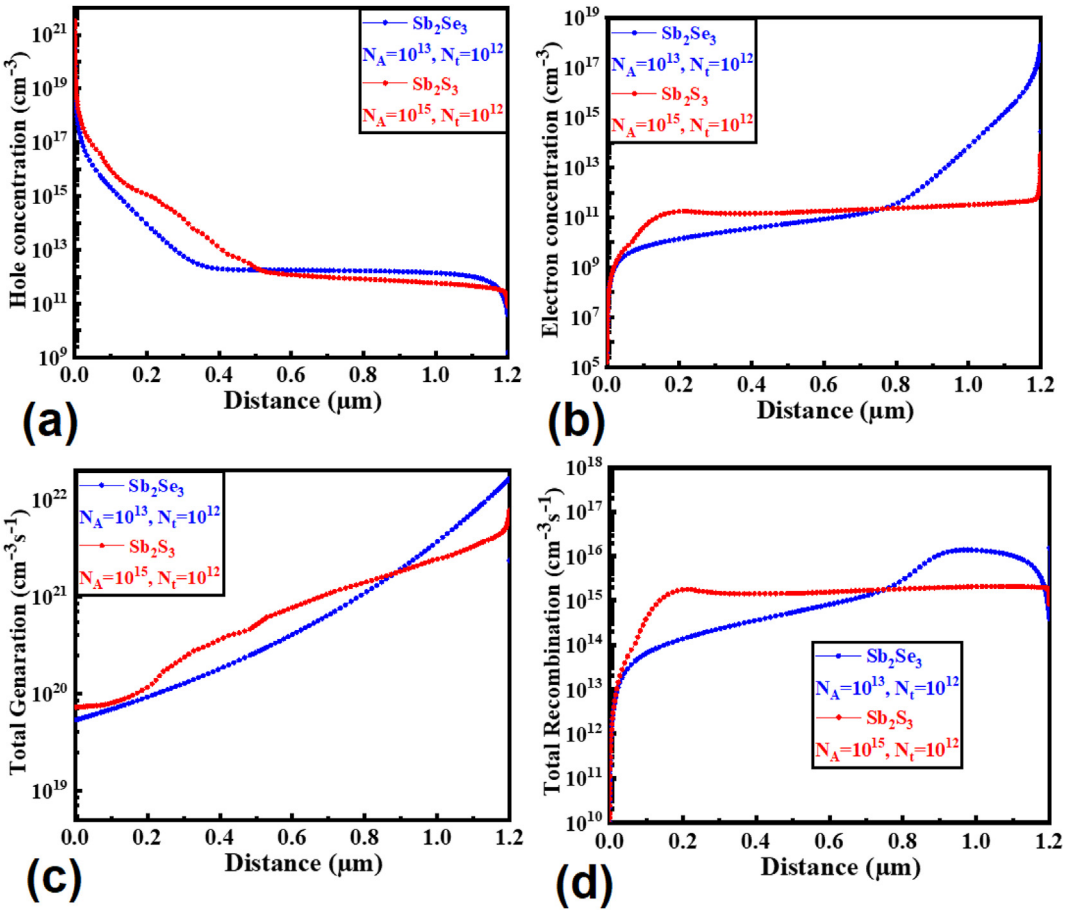

Figure 6. Influence of (a) hole and (b) electron carrier concentration, and total (c) generation and (d) recombination concerning the absorber layer thicknesses.

significantly affected. A detailed study on the impact of bulk and interface defect density has been performed in this section.

3.3.1. Effect of the absorber's bulk defect density

The influence of the bulk defect density of the Sb_2Se_3 and Sb_2S_3 absorber layers on the PV parameters was explored in this section, and the findings are presented in Figure 9.

The carrier recombination rate in the p-type materials can be defined by Eq. (6) [90],

$$\frac{dn}{dt} = -k_3n^3 - k_2n^2 - k_1n \tag{6}$$

where K_3, K_2, and K_1 are the 1st, 2nd, and 3rd order decay constant. Herein, k_i (i = 1,2,3) refers to an interaction between i carriers (electrons/holes/excitons, depending on the species corresponding to the feature). The k_3 represents Auger recombination whereby a third carrier absorbs the energy released from a recombination event and so on, k_2 represents bimolecular recombination with exciton-exciton annihilation, k_1 corresponds either recombination of excitons or recombination between a free carrier and a trapped (localized) carrier [91]. The maximum power loss in the solar cell is due to the non-radiative SRH recombination process [90,92,93] and the defects in the absorber layer mostly cause the SRH recombination, which is generally defined by Eq. (7),

$$R_{SRH} = \frac{np - n_i^2}{\tau\left(p + n - 2n_i\cosh\left(\frac{E_i - E_t}{kT}\right)\right)} \tag{7}$$

where τ, E_t, k, and T represent the charge carrier lifetime, defect energy level within the bandgap, Boltzmann constant, and solar cell operating temperature, respectively. However, carrier lifetime (τ) has been calculated using the following Eq. (8) [76],

$$\tau = \frac{1}{\sigma \times N_t \times V_{th}} \tag{8}$$

where σ, N_t, and V_{th} represent the capture cross-section area of the charge carrier, defect concentration, and charge carrier thermal velocity, respectively.

In Figure 9, the PCE is almost unchanged with a defect density of 10^{13} cm^{-3} and 10^{12} cm^{-3} for the Sb_2Se_3 and Sb_2S_3-based devices. The FF, V_{OC}, and J_{SC} decreased noticeably, and consequently, the PCE decreased from 28 to 18% and from 27 to 19% in Sb_2Se_3 and Sb_2S_3-based solar cells corresponding to defect density of 10^{10}–10^{16} cm^{-3}. Higher SRH-recombination rate is dominant at a defect density of $\geq 10^{13}$ cm^{-3} which deteriorates the cell performance markedly [67]. Thus, a defect density level of $< 10^{13}$ cm^{-3} is required to achieve the highest cell performance.

3.3.2. Effect of the WS_2 ETL's bulk defect density

Figure 10 shows the impacts of ETL's bulk defect density on the solar cell's parameters in the range of 10^{10}– 10^{20} cm^{-3}, while all other parameters remained unchanged as summarized in Tables 1 and 2. It's worth noting that the PV performance metrics of both solar cells degrade noticeably with increased ETL defects. Even though the values of the designed two solar cells' cell parameters are different in magnitude, the trend of lowering the cell performance is very similar to an increase in defects level. Although the PCE retains constant at the highest value up to 10^{18} cm^{-3}, it decreases linearly from ~28 to ~18% and from ~27.0 to ~19% when the defect increases from 10^{18} to 10^{20} cm^{-3}. Thus, the defect

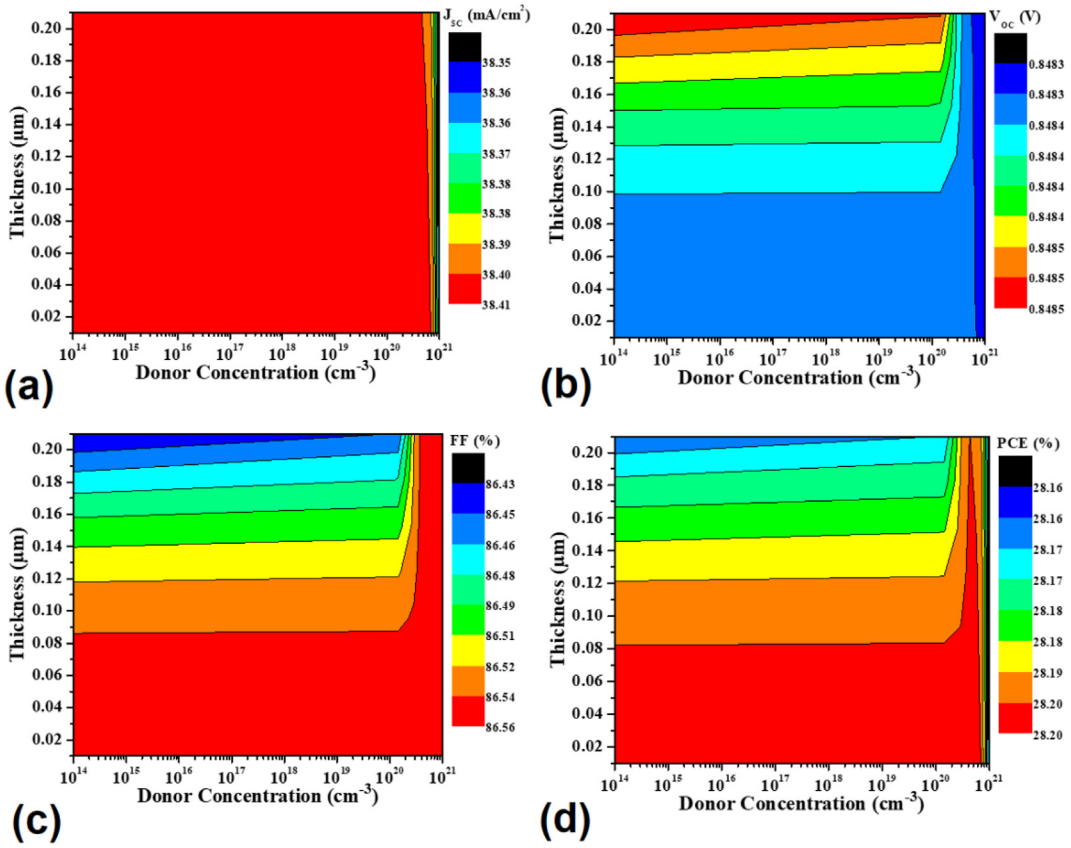

Figure 7. Impact of thickness and doping concentration of WS_2 ETL on the photovoltaic performance (a) J_{sc}, (b) V_{oc}, (c) FF, and (d) PCE of Sb_2Se_3-based solar cell.

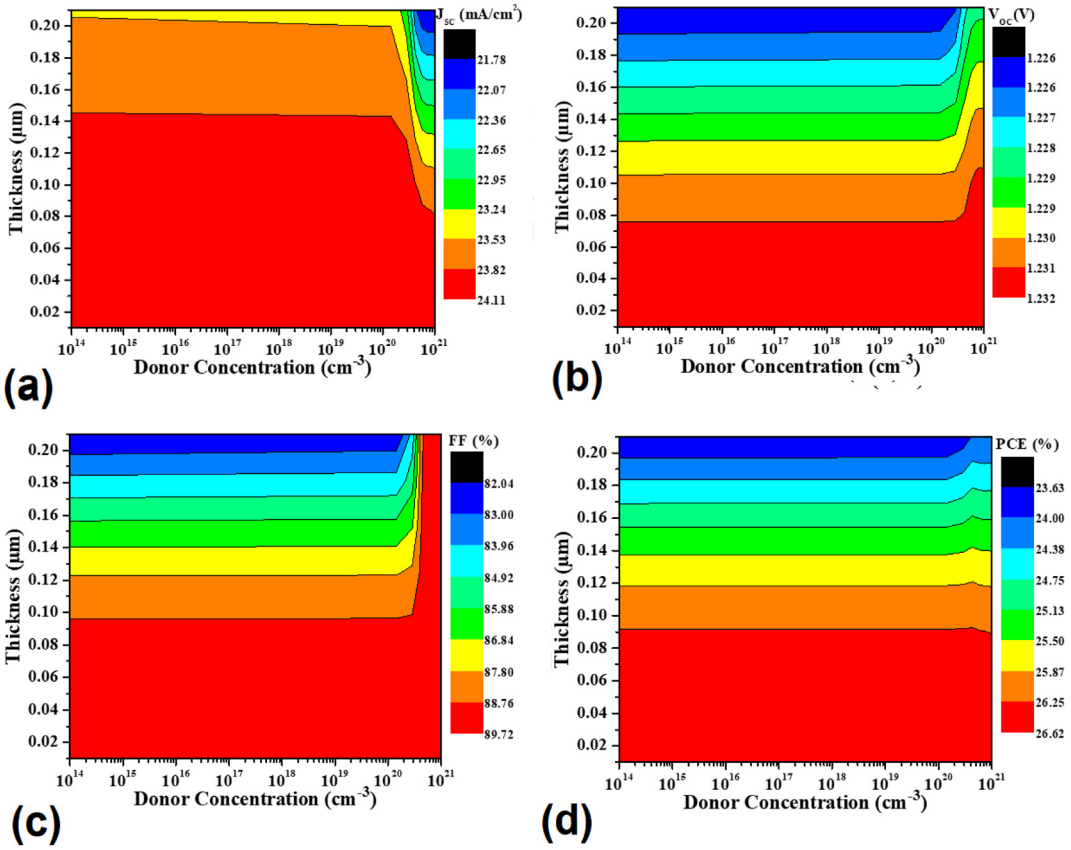

Figure 8. Impact of thickness and doping concentration of WS_2 ETL on the photovoltaic performance (a) J_{sc}, (b) V_{oc}, (c) FF, and (d) PCE of Sb_2S_3-based solar cell.

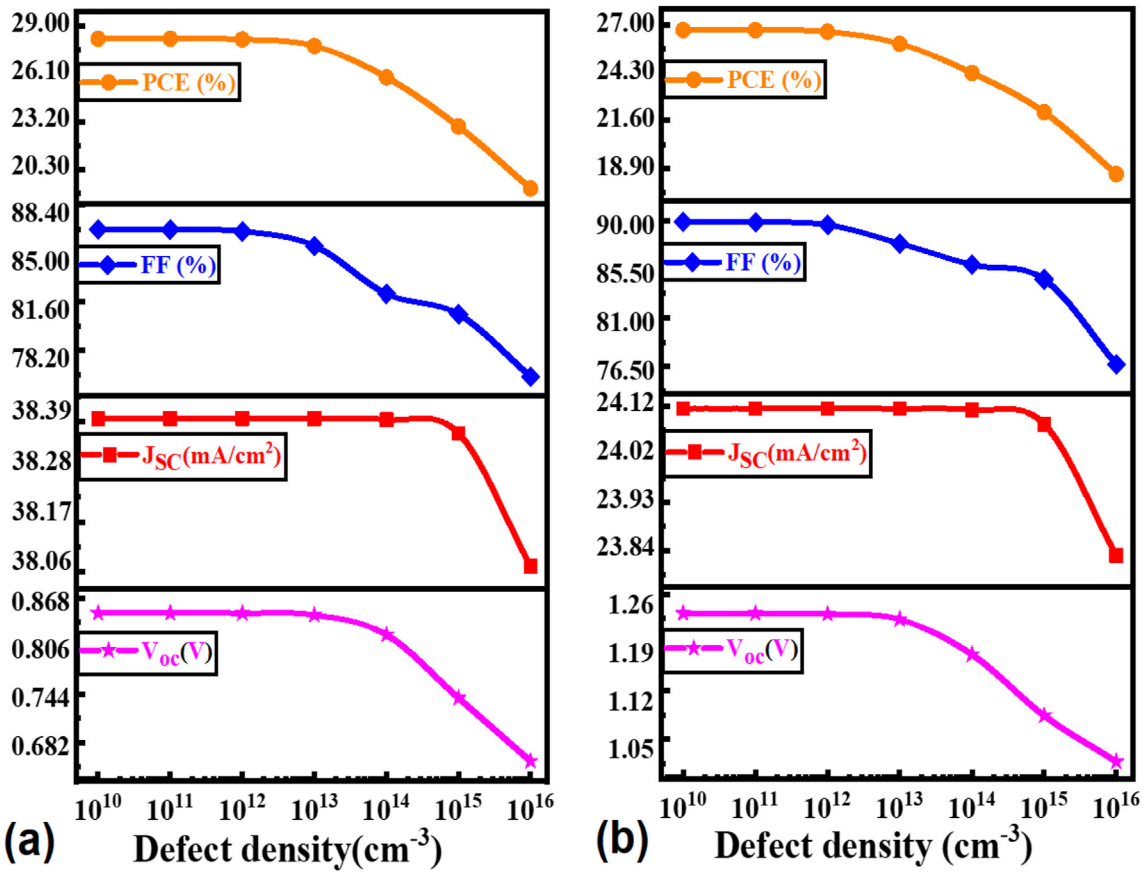

Figure 9. Impact of the bulk defect density of (a) Sb_2Se_3, and (b) Sb_2S_3 absorber layer on the photovoltaic performance.

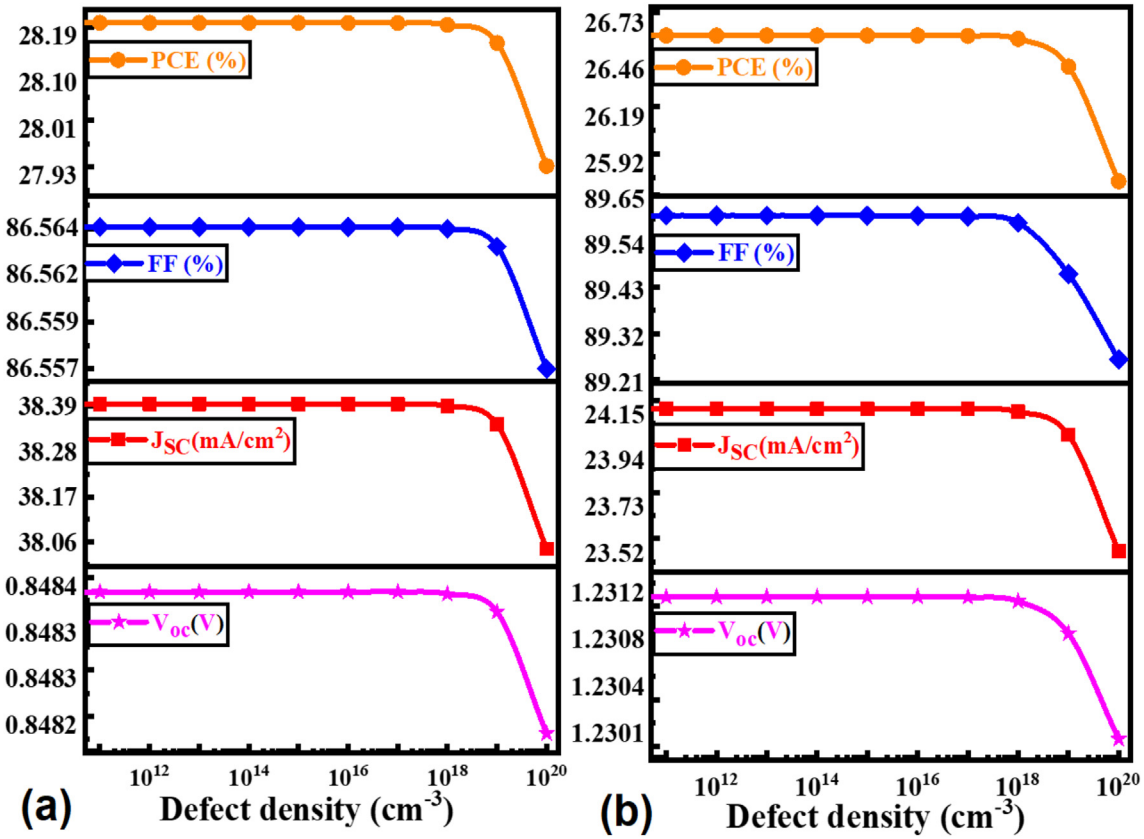

Figure 10. Impact of the WS_2 ETL bulk defect density on the photovoltaic performance of (a) Sb_2Se_3, and (b) Sb_2S_3 solar cells.

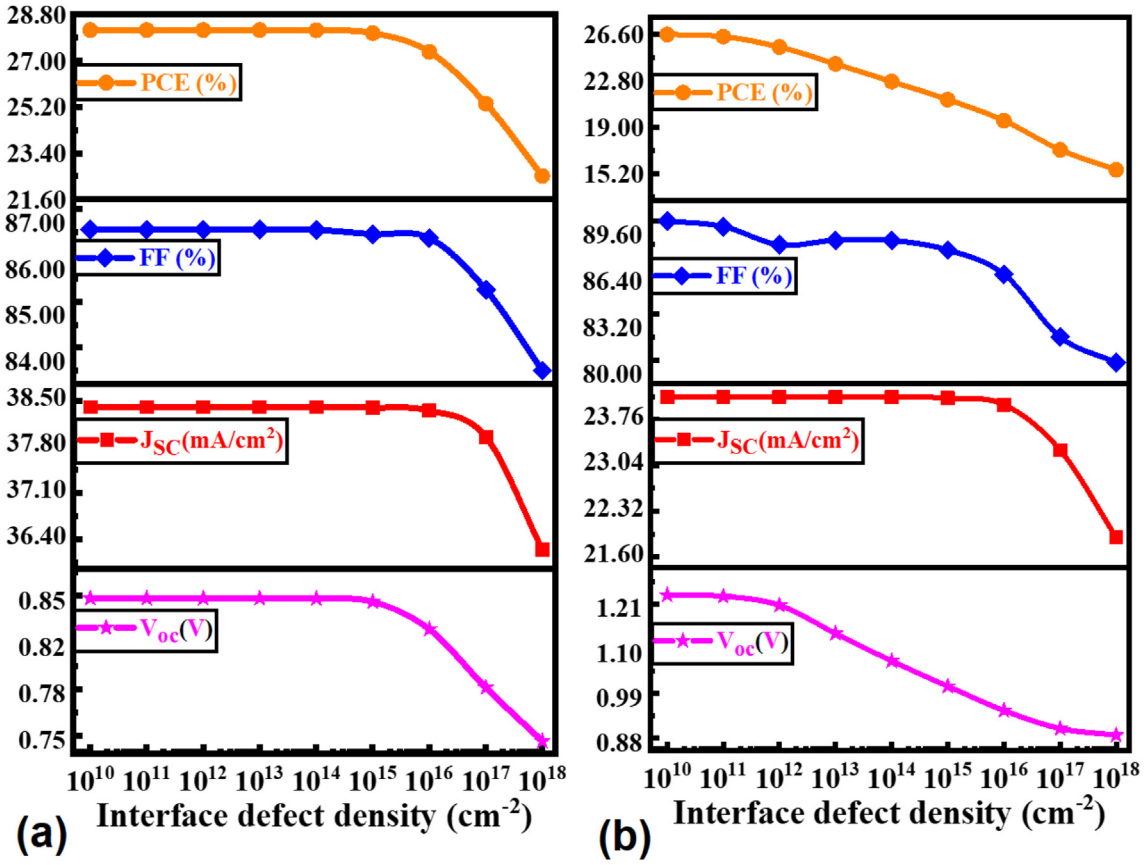

Figure 11. Influence of the ETL/absorber interface defect density on the device performance of (a) Sb_2Se_3, and (b) Sb_2S_3 solar cells.

density is required to be 10^{18} cm^{-3} for achieving the highest cell performance.

3.3.3. *Effect of the ETL/absorber interface defect density*

Figure 11 demonstrate the influence of the interface defect density of the ETL/absorber interface on device performance at the defect density of 10^{10}–10^{18} cm^{-2} at a WT of 300 K, at an unchanged other parameters value as described in Tables 1 and 2.

The impact of defect density on cell performance is almost negligible until the interface defect density reaches 10^{15} cm^{-2} for the WS_2/Sb_2Se_3 interface and 10^{11} cm^{-3} for the WS_2/Sb_2S_3 interface. As perceived from Figure 11, the interface of the Sb_2S_3 solar cell has a more critical impact on the PV characteristics than the Sb_2Se_3 solar cell beyond these marginal values in both devices. All of the metrics drop dramatically as their charge carriers recombine notably with the opposing charge carriers before reaching the junction and at a lower rate of creating EHPs [6,81].

In addition, the effect of temperature variation of Sb_2Se_3 and Sb_2S_3 based heterojunction solar cell is shown in Figure S1. It has been revealed that at high temperatures, the efficiency of Sb_2Se_3 and Sb_2S_3 based heterojunction solar cell reduces, which is consistent with the reported works as well [94].

3.4. *The J-V and QE spectra of the optimized solar cells*

The current density-voltage (J- V) curve and the corresponding QE spectrum as a function of the light wavelength of the optimized HJSCs

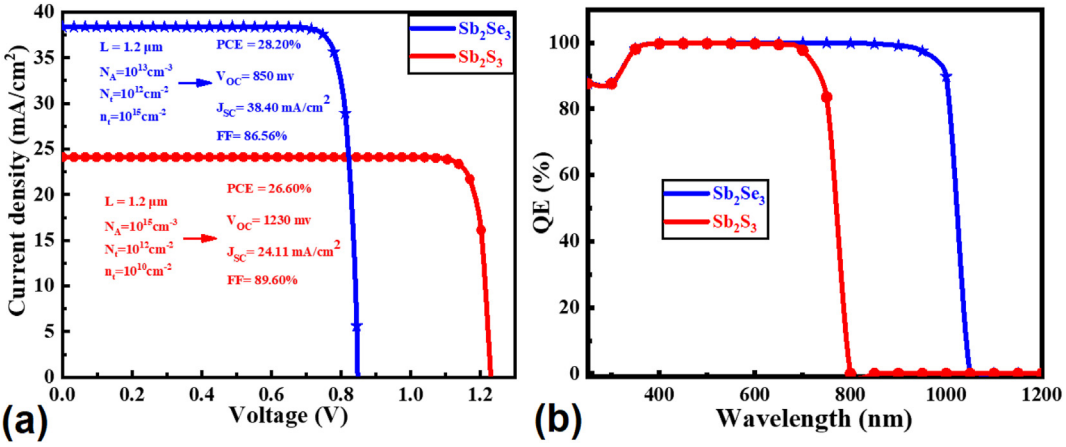

Figure 12. The (a) J-V characteristics, and (b) QE spectra of the proposed Sb_2Se_3 and Sb_2S_3 heterojunction solar cells.

Table 3. Optimized PV parameters of the proposed HJSCs with comparison to similar HJSCs in the literature. [Theo. = Theoretical SQ limit, Exp. = Experimental, Sim. = Simulation].

Absorber material	Types	Junction Formed	J_{SC} (mA/cm^2)	V_{OC} (mV)	FF (%)	PCE (%)	Ref.
Sb_2Se_3	Theo.	Homo	39.99	935	87.70	32.74	[95]
	Exp.	Hetero	30.80	423	58.10	7.50	[96]
	Exp.	Hetero	32.58	400	70.30	9.20	[97]
	Exp.	Hetero	30.86	488	67.19	10.12	[98]
	Sim.	Hetero	38.15	410	74.08	11.52	[65]
	Sim.	Hetero	38.40	850	86.56	28.20	*
Sb_2S_3	Theo.	Homo	25.47	1309	90.50	30.14	[95]
	Exp.	Hetero	14.73	645	65.69	6.27	[61]
	Exp.	Hetero	15.29	748	57.07	6.53	[64]
	Sim.	Hetero	23.73	970	72.32	16.65	[24]
	Sim.	Hetero	24.00	1230	89.60	26.60	*

* This work.

are shown in Figure 12. In Figure 12(a), the simulation results of voltage (V_{OC}), current (J_{SC}), fill factor (FF) and efficiency (η) of the optimized Sb_2Se_3 (Sb_2S_3) proposed solar cells is 850 mV (1230 mV), 38.40 mA/cm^2 (26.60 mA/cm^2), 86.56% (89.60%) and 28.20% (24.11%), respectively. Figure 12(b) reveals that the QE of the Sb_2Se_3 (Sb_2S_3) structure falls to almost 0% at the wavelength of 800 nm (1050 nm), while it is over 97% at a lower value of these wavelength values for Sb_2Se_3 and Sb_2S_3 HJSCs. The degree of current improvement depends on the band gap of the absorber material, reversely, the value of V_{oc} enhanced due to the generation of high built-in potential at the absorber interface, therefore, having an almost ideal band gap for absorbing visible spectra significantly, Sb_2Se_3 and Sb_2S_3 appeal great attention for the fabrication of high-efficiency HJSCs [59,65,67].

Table 3 compares PV performance to previously report experimental and simulation studies. The simulation may be easily verified because the results are consistent with prior studies and are within the SQ limit for single-junction solar cells. Both solar cells proposed here, however, outperform the devices proposed previously [24,61,64–67].

4. Conclusions

The sb-chalcogenides of Sb_2Se_3 and Sb_2S_3-based high-efficiency HJSCs with WS_2 ETL were investigated numerically using SCAPS-1D solar cell simulator. While comprehensive optimization research was carried out, their photovoltaic performance was compared to that found in the literature. The highest PCE of 28.20% with V_{OC} of 850 mV, J_{SC} of 38.40 mA/cm^2, and FF of 86.56% was obtained from Sb_2Se_3 absorber-based heterostructure, while the highest PCE of 26.60% with V_{OC} of 1230 mV, J_{SC} of 26.60 mA/cm^2, and FF of 89.60% was obtained from Sb_2S_3 absorber based heterostructure together with WS_2 ETL layer. Simulation results indicate that WS_2 could be a competitive ETL for fabricating low-toxicity, cost-effective, and highly efficient Sb_2Se_3 and Sb_2S_3-based HJSCs for harnessing solar energy. Furthermore, these devices' higher performance compared with previous reports reveals the high potentiality of Sb-chalcogenide as an absorber material that could be efficient one to realize both high-efficiency high-current (HEHC) and high-efficiency high-voltage (HEHV) solar panels.

Declarations

Author contribution statement

Md. Ferdous Rahman: Conceived and designed the experiments; Performed the experiments; contributed reagents, materials, analysis tools or data; analyzed and interpreted the data; wrote the paper.

Md. Mahabub Alam Moon, Md. Hasan Ali, Md. Dulal Haque, Abdul Kuddus, Jaker Hossain and Abu Bakar Md. Ismail: analyzed and interpreted the data; wrote the paper.

M. Khalid Hossain: Conceived and designed the experiments; analyzed and interpreted the data; wrote the paper.

Funding statement

Prof. Dr. Md. Ferdous Rahman was partially supported by an innovation fund from the ICT Division, Govt. of Bangladesh [Grant No. 22IF15426 (2021–2022)].

Data availability statement

Data will be made available on request.

Declaration of interest's statement

The authors declare no conflict of interest.

Additional information

Supplementary content related to this article has been published online at https://doi.org/10.1016/j.heliyon.2022.e12034.

Acknowledgments

The authors are thankful to Marc Burgleman and his colleagues at the University of Electronics and Information Systems (ELIS), Department of Electronics and Information Systems, Belgium, for supplying the SCAPS software package, version 3.3.07.

References

[1] X. Wang, R. Tang, C. Wu, C. Zhu, T. Chen, Development of antimony sulfide–selenide $Sb_2(S, Se)_3$-based solar cells, J. Energy Chem. 27 (2018) 713–721.
[2] M.K. Hossain, G.A. Raihan, M.A. Akbar, M.H. Kabir Rubel, M.H. Ahmed, M.I. Khan, S. Hossain, S.K. Sen, M.I.E. Jalal, A. El-Denglawey, Current applications and future potential of rare earth oxides in sustainable nuclear, radiation, and energy devices: a review, ACS Appl. Electron. Mater. 4 (2022) 3327–3353.
[3] M.A. Green, How did solar cells get so cheap? Joule 3 (2019) 631–633.
[4] M.K. Hossain, M.F. Pervez, S. Tayyaba, M.J. Uddin, A.A. Mortuza, M.N.H. Mia, M.S. Manir, M.R. Karim, M.A. Khan, Efficiency enhancement of natural dye sensitized solar cell by optimizing electrode fabrication parameters, Mater. Sci. 35 (2017) 816–823.
[5] M.K. Hossain, M.F. Pervez, M.N.H. Mia, A.A. Mortuza, M.S. Rahaman, M.R. Karim, J.M.M. Islam, F. Ahmed, M.A. Khan, Effect of dye extracting solvents and sensitization time on photovoltaic performance of natural dye sensitized solar cells, Results Phys. 7 (2017) 1516–1523.
[6] S.R.I. Biplab, M.H. Ali, M.M.A. Moon, M.F. Pervez, M.F. Rahman, J. Hossain, Performance enhancement of CIGS-based solar cells by incorporating an ultrathin $BaSi_2$ BSF layer, J. Comput. Electron. 19 (2020) 342–352.
[7] M.K. Hossain, A.A. Mortuza, S.K. Sen, M.K. Basher, M.W. Ashraf, S. Tayyaba, M.N.H. Mia, M.J. Uddin, A comparative study on the influence of pure anatase and Degussa-P25 TiO_2 nanomaterials on the structural and optical properties of dye sensitized solar cell (DSSC) photoanode, Optik 171 (2018) 507–516.
[8] M.K. Hossain, M.F. Pervez, M.J. Uddin, S. Tayyaba, M.N.H. Mia, M.S. Bashar, M.K.H. Jewel, M.A.S. Haque, M.A. Hakim, M.A. Khan, Influence of natural dye adsorption on the structural, morphological and optical properties of TiO_2 based photoanode of dye-sensitized solar cell, Mater. Sci. 36 (2017) 93–101.
[9] S. Sen, S. Ganguly, A. Das, J. Sen, S. Dey, Renewable energy scenario in India: opportunities and challenges, J. Afr. Earth Sci. 122 (2016) 25–31.
[10] W. Qarony, M.I. Hossain, M.K. Hossain, M.J. Uddin, A. Haque, A.R. Saad, Y.H. Tsang, Efficient amorphous silicon solar cells: characterization, optimization, and optical loss analysis, Results Phys. 7 (2017) 4287–4293.
[11] M.I. Hossain, W. Qarony, M.K. Hossain, M.K. Debnath, M.J. Uddin, Y.H. Tsang, Effect of back reflectors on photon absorption in thin-film amorphous silicon solar cells, Appl. Nanosci. 7 (2017) 489–497.
[12] M.K. Basher, R. Mishan, S. Biswas, M.K. Hossain, M.A.R. Akand, M.A. Matin, Study and analysis the Cu nanoparticle assisted texturization forming low reflective silicon surface for solar cell application, AIP Adv. 9 (2019), 075118.
[13] M.K. Basher, M.K. Hossain, M.J. Uddin, M.A.R. Akand, K.M. Shorowordi, Effect of pyramidal texturization on the optical surface reflectance of monocrystalline photovoltaic silicon wafers, Optik 172 (2018) 801–811.
[14] S. Biswas, M.K. Basher, M.K. Hossain, M.A.R. Akand, M.T. Rahman, M.R. Ahmed, M.A. Matin, S. Huque, Study and analysis of the morphological, elemental and

electrical properties of phosphorus doped monocrystalline silicon solar cell, Mater. Res. Express 6 (2019), 055515.
[15] M.K. Basher, M.J. Uddin, M.K. Hossain, M.A.R. Akand, S. Biswas, M.N.H. Mia, K.M. Shorowordi, Effect of doping profile on sheet resistance and contact resistance of monocrystalline silicon solar cells, Mater. Res. Express 6 (2019), 085510.
[16] M.K.K. Hossain, M.F.F. Pervez, M.N.H.N.H. Mia, S. Tayyaba, M.J.J. Uddin, R. Ahamed, R.A.A. Khan, M. Hoq, M.A.A. Khan, F. Ahmed, Annealing temperature effect on structural, morphological and optical parameters of mesoporous TiO_2 film photoanode for dye-sensitized solar cell application, Mater. Sci. 35 (2017) 868–877.
[17] M.K. Hossain, M.T. Rahman, M.K. Basher, M.S. Manir, M.S. Bashar, Influence of thickness variation of gamma-irradiated DSSC photoanodic TiO_2 film on structural, morphological and optical properties, Optik 178 (2019) 449–460.
[18] M.K. Hossain, M.T. Rahman, M.K. Basher, M.J. Afzal, M.S. Bashar, Impact of ionizing radiation doses on nanocrystalline TiO_2 layer in DSSC's photoanode film, Results Phys. 11 (2018) 1172–1181.
[19] A.M. Ganose, C.N. Savory, D.O. Scanlon, Beyond methylammonium lead iodide: prospects for the emergent field of ns 2 containing solar absorbers, Chem. Commun. 53 (2017) 20–44.
[20] V.V. Tyagi, N.A.A. Rahim, N.A. Rahim, J.A./L. Selvaraj, Progress in solar PV technology: research and achievement, Renew. Sustain. Energy Rev. 20 (2013) 443–461.
[21] M. Hosenuzzaman, N.A. Rahim, J. Selvaraj, M. Hasanuzzaman, A.B.M.A. Malek, A. Nahar, Global prospects, progress, policies, and environmental impact of solar photovoltaic power generation, Renew. Sustain. Energy Rev. 41 (2015) 284–297.
[22] H. Bencherif, F. Meddour, M.H. Elshorbagy, M. Khalid Hossain, A. Cuadrado, M.A. Abdi, T. Bendib, S. Kouda, J. Alda, Performance enhancement of $(FAPbI_3)_{1-x}(MAPbBr_3)_x$ perovskite solar cell with an optimized design, Micro and Nanostructures 171 (2022), 207403.
[23] F.H. Alharbi, S. Kais, Theoretical limits of photovoltaics efficiency and possible improvements by intuitive approaches learned from photosynthesis and quantum coherence, Renew. Sustain. Energy Rev. 43 (2015) 1073–1089.
[24] M.A. Green, Y. Hishikawa, E.D. Dunlop, D.H. Levi, J. Hohl-Ebinger, A.W.Y. Ho-Baillie, Solar cell efficiency tables (version 51), Prog. Photovoltaics Res. Appl. 26 (2018) 3–12.
[25] P. Jackson, R. Wuerz, D. Hariskos, E. Lotter, W. Witte, M. Powalla, Effects of heavy alkali elements in $Cu(In,Ga)Se_2$ solar cells with efficiencies up to 22.6, Phys. Status Solidi Rapid Res. Lett. 10 (2016) 583–586.
[26] A. Zakutayev, Brief review of emerging photovoltaic absorbers, Curr. Opin. Green Sustain. Chem. 4 (2017) 8–15.
[27] M.F. Rahman, M.J.A. Habib, M.H. Ali, M.H.K. Rubel, M.R. Islam, A.B.M. Ismail, M.K. Hossain, Design and numerical investigation of cadmium telluride (CdTe) and iron silicide ($FeSi_2$) based double absorber solar cells to enhance power conversion efficiency, AIP Adv. 12 (2022), 105317.
[28] J. Chantana, H. Uegaki, T. Minemoto, Influence of Na in Cu_2SnS_3 film on its physical properties and photovoltaic performances, Thin Solid Films 636 (2017) 431–437.
[29] X. Jin, L. Zhang, G. Jiang, W. Liu, C. Zhu, High open-circuit voltage of ternary Cu_2GeS_3 thin film solar cells from combustion synthesized Cu-Ge alloy, Sol. Energy Mater. Sol. Cells 160 (2017) 319–327.
[30] M. Umehara, Y. Takeda, T. Motohiro, T. Sakai, H. Awano, R. Maekawa, $Cu_2Sn_{1-x}Ge_xS_3$ (x=0.17) thin-film solar cells with high conversion efficiency of 6.0, APEX 6 (2013), 045501.
[31] D.-J. Xue, S.-C. Liu, C.-M. Dai, S. Chen, C. He, L. Zhao, J.-S. Hu, L.-J. Wan, GeSe thin-film solar cells fabricated by self-regulated rapid thermal sublimation, J. Am. Chem. Soc. 139 (2017) 958–965.
[32] W. Septina, S. Ikeda, Y. Iga, T. Harada, M. Matsumura, Thin film solar cell based on $CuSbS_2$ absorber fabricated from an electrochemically deposited metal stack, Thin Solid Films 550 (2014) 700–704.
[33] D.-J. Xue, B. Yang, Z.-K. Yuan, G. Wang, X. Liu, Y. Zhou, L. Hu, D. Pan, S. Chen, J. Tang, $CuSbSe_2$ as a potential photovoltaic absorber material: studies from theory to experiment, Adv. Energy Mater. 5 (2015), 1501203.
[34] S. Hartnauer, S. Körbel, M.A.L. Marques, S. Botti, P. Pistor, R. Scheer, Research update: stable single-phase Zn-rich $Cu_2ZnSnSe_4$ through in doping, Apl. Mater. 4 (2016), 070701.
[35] L. Luo, W. Luan, B. Yuan, C. Zhang, L. Jin, High efficient and stable solid solar cell: based on FeS2 nanocrystals and P3HT: PCBM, Energy Proc. 75 (2015) 2181–2186.
[36] M.M.A. Moon, M.H. Ali, M.F. Rahman, J. Hossain, A.B.M. Ismail, Design and simulation of $FeSi_2$-based novel heterojunction solar cells for harnessing visible and near-infrared light, Phys. Status Solidi 217 (2020), 1900921.
[37] T.M. Razykov, G.S. Boltaev, A. Bosio, B. Ergashev, K.M. Kouchkarov, N.K. Mamarasulov, A.A. Mavlonov, A. Romeo, N. Romeo, O.M. Tursunkulov, R. Yuldoshov, Characterisation of SnSe thin films fabricated by chemical molecular beam deposition for use in thin film solar cells, Sol. Energy 159 (2018) 834–840.
[38] R. Tang, Z.-H. Zheng, Z.-H. Su, X.-J. Li, Y.-D. Wei, X.-H. Zhang, Y.-Q. Fu, J.-T. Luo, P. Fan, G.-X. Liang, Highly efficient and stable planar heterojunction solar cell based on sputtered and post-selenized Sb_2Se_3 thin film, Nano Energy 64 (2019), 103929.
[39] R. Tang, X. Wang, C. Jiang, S. Li, G. Jiang, S. Yang, C. Zhu, T. Chen, Vacuum assisted solution processing for highly efficient Sb_2S_3 solar cells, J. Mater. Chem. A. 6 (2018) 16322–16327.
[40] S. Lu, Y. Zhao, C. Chen, Y. Zhou, D. Li, K. Li, W. Chen, X. Wen, C. Wang, R. Kondrotas, N. Lowe, J. Tang, Sb_2Se_3 thin-film photovoltaics using aqueous solution sprayed SnO_2 as the buffer layer, Adv. Electron. Mater. 4 (2018), 1700329.
[41] S. Chen, T. Liu, Z. Zheng, M. Ishaq, G. Liang, P. Fan, T. Chen, J. Tang, Recent progress and perspectives on Sb_2Se_3-based photocathodes for solar hydrogen production via photoelectrochemical water splitting, J. Energy Chem. 67 (2022) 508–523.
[42] G.-X. Liang, Y.-D. Luo, S. Chen, R. Tang, Z.-H. Zheng, X.-J. Li, X.-S. Liu, Y.-K. Liu, Y.-F. Li, X.-Y. Chen, Z.-H. Su, X.-H. Zhang, H.-L. Ma, P. Fan, Sputtered and selenized Sb_2Se_3 thin-film solar cells with open-circuit voltage exceeding 500 mV, Nano Energy 73 (2020), 104806.
[43] Y.-D. Luo, R. Tang, S. Chen, J.-G. Hu, Y.-K. Liu, Y.-F. Li, X.-S. Liu, Z.-H. Zheng, Z.-H. Su, X.-F. Ma, P. Fan, X.-H. Zhang, H.-L. Ma, Z.-G. Chen, G.-X. Liang, An effective combination reaction involved with sputtered and selenized Sb precursors for efficient Sb_2Se_3 thin film solar cells, Chem. Eng. J. 393 (2020), 124599.
[44] S. Chen, T. Liu, M. Chen, M. Ishaq, R. Tang, Z. Zheng, Z. Su, X. Li, X. Qiao, P. Fan, G. Liang, Crystal growth promotion and interface optimization enable highly efficient Sb_2Se_3 photocathodes for solar hydrogen evolution, Nano Energy 99 (2022), 107417.
[45] C. Chen, W. Li, Y. Zhou, C. Chen, M. Luo, X. Liu, K. Zeng, B. Yang, C. Zhang, J. Han, J. Tang, Optical properties of amorphous and polycrystalline Sb_2Se_3 thin films prepared by thermal evaporation, Appl. Phys. Lett. 107 (2015), 043905.
[46] M.B. Costa, F.W. de Souza Lucas, L.H. Mascaro, Thermal treatment effects on electrodeposited Sb 2 Se 3 photovoltaic thin films, Chemelectrochem 4 (2017) 2507–2514.
[47] Y. Lai, Z. Chen, C. Han, L. Jiang, F. Liu, J. Li, Y. Liu, Preparation and characterization of Sb_2Se_3 thin films by electrodeposition and annealing treatment, Appl. Surf. Sci. 261 (2012) 510–514.
[48] Y. Zhou, M. Leng, Z. Xia, J. Zhong, H. Song, X. Liu, B. Yang, J. Zhang, J. Chen, K. Zhou, J. Han, Y. Cheng, J. Tang, Solution-processed antimony selenide heterojunction solar cells, Adv. Energy Mater. 4 (2014), 1301846.
[49] O. Madelung, Semiconductors: Data Handbook, Springer Berlin Heidelberg, Berlin, Heidelberg, 2004.
[50] G.-X. Liang, Z.-H. Zheng, P. Fan, J.-T. Luo, J.-G. Hu, X.-H. Zhang, H.-L. Ma, B. Fan, Z.-K. Luo, D.-P. Zhang, Thermally induced structural evolution and performance of Sb_2Se_3 films and nanorods prepared by an easy sputtering method, Sol. Energy Mater. Sol. Cells 174 (2018) 263–270.
[51] K. Li, R. Kondrotas, C. Chen, S. Lu, X. Wen, D. Li, J. Luo, Y. Zhao, J. Tang, Improved efficiency by insertion of $Zn_{1-x}Mg_xO$ through sol-gel method in ZnO/Sb_2Se_3 solar cell, Sol. Energy 167 (2018) 10–17.
[52] C. Chen, Y. Zhao, S. Lu, K. Li, Y. Li, B. Yang, W. Chen, L. Wang, D. Li, H. Deng, F. Yi, J. Tang, Accelerated optimization of TiO_2/Sb_2Se_3 thin film solar cells by high-throughput combinatorial approach, Adv. Energy Mater. 7 (2017), 1700866.
[53] S. Messina, M.T.S. Nair, P.K. Nair, Antimony selenide absorber thin films in all-chemically deposited solar cells, J. Electrochem. Soc. 156 (2009) H327.
[54] Y. Itzhaik, O. Niitsoo, M. Page, G. Hodes, Sb_2S_3-Sensitized nanoporous TiO_2 solar cells, J. Phys. Chem. C 113 (2009) 4254–4256.
[55] Z. Li, X. Liang, G. Li, H. Liu, H. Zhang, J. Guo, J. Chen, K. Shen, X. San, W. Yu, R.E.I. Schropp, Y. Mai, 9.2%-efficient core-shell structured antimony selenide nanorod array solar cells, Nat. Commun. 10 (2019) 125.
[56] H. Ning, H. Guo, J. Zhang, X. Wang, X. Jia, J. Qiu, N. Yuan, J. Ding, Enhancing the efficiency of Sb_2S_3 solar cells using dual-functional potassium doping, Sol. Energy Mater. Sol. Cells 221 (2021), 110816.
[57] J. Lin, A. Mahmood, G. Chen, N. Ahmad, M. Chen, P. Fan, S. Chen, R. Tang, G. Liang, Crystallographic orientation control and defect passivation for high-efficient antimony selenide thin-film solar cells, Mater, Today Phys 27 (2022), 100772.
[58] R. Tang, S. Chen, Z. Zheng, Z. Su, J. Luo, P. Fan, X. Zhang, J. Tang, G. Liang, Heterojunction annealing enabling record open-circuit voltage in antimony triselenide solar cells, Adv. Mater. 34 (2022), 2109078.
[59] L. Lin, L. Jiang, Y. Qiu, B. Fan, Analysis of Sb_2Se_3/CdS based photovoltaic cell: a numerical simulation approach, J. Phys. Chem. Solid. 122 (2018) 19–24.
[60] F. Baig, Y.H. Khattak, S. Beg, B.M. Soucase, Numerical analysis of a novel CNT/$Cu_2O/Sb_2Se_3/In_2S_3$/ITO antimony selenide solar cell, Optik 197 (2019), 163107.
[61] I. Gharibshahian, A.A. Orouji, S. Sharbati, Alternative buffer layers in Sb_2Se_3 thin-film solar cells to reduce open-circuit voltage offset, Sol. Energy 202 (2020) 294–303.
[62] Y. Xiao, H. Wang, H. Kuang, Numerical simulation and performance optimization of Sb_2S_3 solar cell with a hole transport layer, Opt. Mater. 108 (2020), 110414.
[63] Y. Cao, X. Zhu, H. Chen, X. Zhang, J. Zhouc, Z. Hu, J. Pang, Towards high efficiency inverted Sb_2Se_3 thin film solar cells, Sol. Energy Mater. Sol. Cells 200 (2019), 109945.
[64] I. Gharibshahian, A.A. Orouji, S. Sharbati, Towards high efficiency Cd-Free Sb_2Se_3 solar cells by the band alignment optimization, Sol. Energy Mater. Sol. Cells 212 (2020), 110581.
[65] Z.-Q. Li, M. Ni, X.-D. Feng, Simulation of the Sb_2Se_3 solar cell with a hole transport layer, Mater. Res. Express 7 (2020), 016416.
[66] F. Baig, Y.H. Khattak, A. Shuja, K. Riaz, B.M. Soucase, Performance investigation of Sb_2Se_3 based solar cell by device optimization, band offset engineering and Hole Transport Layer in SCAPS-1D, Curr. Appl. Phys. 20 (2020) 973–981.
[67] A. Basak, U.P. Singh, Numerical modelling and analysis of earth abundant Sb_2S_3 and Sb_2Se_3 based solar cells using SCAPS-1D, Sol. Energy Mater. Sol. Cells 230 (2021), 111184.
[68] M.F. Rahman, J. Hossain, A. Kuddus, S. Tabassum, M.H.K. Rubel, M.M. Rahman, Y. Moriya, H. Shirai, A.B.M. Ismail, A novel CdTe ink-assisted direct synthesis of CdTe thin films for the solution-processed CdTe solar cells, J. Mater. Sci. 55 (2020) 7715–7730.
[69] M.M.A. Moon, M.F. Rahman, M. Kamruzzaman, J. Hossain, A.B.M. Ismail, Unveiling the prospect of a novel chemical route for synthesizing solution-processed CdS/CdTe thin-film solar cells, Energy Rep. 7 (2021) 1742–1756.
[70] M.K.S. Bin Rafiq, N. Amin, H.F. Alharbi, M. Luqman, A. Ayob, Y.S. Alharthi, N.H. Alharthi, B. Bais, M. Akhtaruzzaman, WS_2: a new window layer material for solar cell application, Sci. Rep. 10 (2020) 771.

[71] M. Burgelman, P. Nollet, S. Degrave, Modelling polycrystalline semiconductor solar cells, Thin Solid Films 361–362 (2000) 527–532.
[72] K. Decock, P. Zabierowski, M. Burgelman, Modeling metastabilities in chalcopyrite-based thin film solar cells, J. Appl. Phys. 111 (2012), 043703.
[73] E. Fortunato, D. Ginley, H. Hosono, D.C. Paine, Transparent conducting oxides for photovoltaics, MRS Bull. 32 (2007) 242–247.
[74] R.G. Gordon, Criteria for choosing transparent conductors, MRS Bull. 25 (2000) 52–57.
[75] J. Zhang, R. Kondrotas, S. Lu, C. Wang, C. Chen, J. Tang, Alternative back contacts for Sb_2Se_3 solar cells, Sol. Energy 182 (2019) 96–101.
[76] M. Burgelman, K. Decock, A. Niemegeers, J. Verschraegen, S. Degrave, SCAPS Manual, Univ. Gent., 2019, pp. 1–111.
[77] K. Sobayel, M. Akhtaruzzaman, K.S. Rahman, M.T. Ferdaous, Z.A. Al-Mutairi, H.F. Alharbi, N.H. Alharthi, M.R. Karim, S. Hasmady, N. Amin, A comprehensive defect study of tungsten disulfide (WS_2) as electron transport layer in perovskite solar cells by numerical simulation, Results Phys. 12 (2019) 1097–1103.
[78] K. Sobayel, K.S. Rahman, M.R. Karim, M.O. Aijaz, M.A. Dar, M.A. Shar, H. Misran, N. Amin, Numerical modeling on prospective buffer layers for tungsten di-sulfide (WS_2) solar cells by scaps-1D, Chalcogenide Lett. 15 (2018) 307–315.
[79] H. Bencherif, M.K. Hossain, Design and numerical investigation of efficient $(FAPbI_3)_{1-x}(CsSnI_3)_x$ perovskite solar cell with optimized performances, Sol. Energy 248 (2022) 137–148.
[80] M.K. Hossain, M.H.K. Rubel, G.F.I. Toki, I. Alam, M.F. Rahman, H. Bencherif, Effect of various electron and hole transport layers on the performance of $CsPbI_3$-based perovskite solar cells: a numerical investigation in DFT, SCAPS-1D, and wxAMPS frameworks, ACS Omega 7 (2022) 43210–43230.
[81] M.M.A. Moon, M.H. Ali, M.F. Rahman, A. Kuddus, J. Hossain, A.B.M. Ismail, Investigation of thin-film p -$BaSi_2$/n-CdS heterostructure towards semiconducting silicide based high efficiency solar cell, Phys. Scripta 95 (2020), 035506.
[82] S.H. Zyoud, A.H. Zyoud, N.M. Ahmed, A.R. Prasad, S.N. Khan, A.F.I. Abdelkader, M. Shahwan, Numerical modeling of high conversion efficiency FTO/ZnO/CdS/CZTS/MO thin film-based solar cells: using SCAPS-1D software, Crystals 11 (2021) 1468.
[83] Y. Cao, C. Liu, J. Jiang, X. Zhu, J. Zhou, J. Ni, J. Zhang, J. Pang, M.H. Rummeli, W. Zhou, H. Liu, G. Cuniberti, Theoretical insight into high-efficiency triple-junction tandem solar cells via the band engineering of antimony chalcogenides, Sol. RRL. 5 (2021), 2000800.
[84] A.E. Delahoy, Z. Cheng, K.K. Chin, Carrier collection in thin-film CdTe solar cells: theory and experiment, 27th, Eur. Photovolt. Sol. Energy Conf. Exhib. (2012) 2837–2842.
[85] A.E.H. Benzetta, M. Abderrezek, M.E. Djeghlal, A comparative study on generation and recombination process of kesterite CZTS based thin film solar cells for different designs, Optik 219 (2020), 165300.
[86] M. Atowar Rahman, Enhancing the photovoltaic performance of Cd-free Cu_2ZnSnS_4 heterojunction solar cells using SnS HTL and TiO_2 ETL, Sol. Energy 215 (2021) 64–76.
[87] R. El Otmani, A. El Manouni, A. Al Maggoussi, Numerical simulation of CZTSe based solar cells using different back surface field layers: improvement and comparison, J. Electron. Mater. 50 (2021) 2021–2033.
[88] Y.H. Khattak, F. Baig, S. Ullah, B. Marí, S. Beg, H. Ullah, Enhancement of the conversion efficiency of thin film kesterite solar cell, J. Renew. Sustain. Energy 10 (2018), 033501.
[89] R.K. Zahoo, A.N. Saleh, Effect of carrier concentration and thickness of absorber layer on performance CBTS solar cell, Turkish J. Comput. Math. Educ. 12 (2021) 5056–5064.
[90] S. Ahmmed, A. Aktar, S. Tabassum, M.H. Rahman, M.F. Rahman, A.B. Md. Ismail, CuO based solar cell with V_2O_5 BSF layer: theoretical validation of experimental data, Superlattice. Microst. 151 (2021), 106830.
[91] A.G. Barrette, Ultrafast Optical Studies of Amplified Spontaneous Emission in Hybrid Organic-Inorganic Perovskites, North Carolina State University, 2018. http://www.lib.ncsu.edu/resolver/1840.20/35772.
[92] S. Ahmmed, A. Aktar, M.F. Rahman, J. Hossain, A.B.M. Ismail, A numerical simulation of high efficiency CdS/CdTe based solar cell using NiO HTL and ZnO TCO, Optik 223 (2020), 165625.
[93] J. Chen, N. Park, Causes and solutions of recombination in perovskite solar cells, Adv. Mater. 31 (2019), 1803019.
[94] A. Bouich, B. Hartiti, S. Ullah, H. Ullah, M.E. Touhami, D.M.F. Santos, B. Mari, Experimental, theoretical, and numerical simulation of the performance of $CuIn_xGa_{(1-x)}S_2$-based solar cells, Optik 183 (2019) 137–147.
[95] S. Rühle, Tabulated values of the Shockley–Queisser limit for single junction solar cells, Sol. Energy 130 (2016) 139–147.
[96] J.A. Chang, J.H. Rhee, S.H. Im, Y.H. Lee, H. Kim, S. Il Seok, M.K. Nazeeruddin, M. Gratzel, High-performance nanostructured Inorganic−Organic heterojunction solar cells, Nano Lett. 10 (2010) 2609–2612.
[97] S.H. Im, C.-S. Lim, J.A. Chang, Y.H. Lee, N. Maiti, H.-J. Kim, M.K. Nazeeruddin, M. Grätzel, S. Il Seok, Toward interaction of sensitizer and functional moieties in hole-transporting materials for efficient semiconductor-sensitized solar cells, Nano Lett. 11 (2011) 4789–4793.
[98] Z. Duan, X. Liang, Y. Feng, H. Ma, B. Liang, Y. Wang, S. Luo, S. Wang, R.E.I. Schropp, Y. Mai, Z. Li, Sb_2Se_3 thin-film solar cells exceeding 10% power conversion efficiency enabled by injection vapor deposition technology, Adv. Mater. 34 (2022), 2202969.